Electronic and magnetic properties of molecule-metal interfaces: Transition-metal phthalocyanines adsorbed on Ag(100)

A. Mugarza,[1,2] R. Robles,[2] C. Krull,[1,2] R. Korytár,[2,3] N. Lorente,[2] and P. Gambardella[1,2,4,5]

[1]*Catalan Institute of Nanotecnology (ICN), UAB Campus, E-08193 Bellaterra, Spain*

[2]*Centre d'Investigaciò en Nanociència i Nanotecnologia, CIN2, (ICN-CSIC), UAB Campus, E-08193 Bellaterra, Spain*

[3]*Institut für Nanotechnologie, Karlsruher Institut für Technologie, Hermann-von-Helmholtzplatz 1, D-76344 Eggenstein-Leopoldshafen, Germany*

[4]*Institució Catalana de Recerca i Estudis Avancats (ICREA), E-08193 Barcelona, Spain*

[5]*Departament de Física, UAB Campus, E-08193 Barcelona, Spain*

(Received 9 February 2012; revised manuscript received 21 March 2012; published 19 April 2012)

We present a systematic investigation of molecule-metal interactions for transition-metal phthalocyanines (TMPc, with TM = Fe, Co, Ni, Cu) adsorbed on Ag(100). Scanning tunneling spectroscopy and density functional theory provide insight into the charge transfer and hybridization mechanisms of TMPc as a function of increasing occupancy of the 3*d* metal states. We show that all four TMPc receive approximately one electron from the substrate. Charge transfer occurs from the substrate to the molecules, inducing a charge reorganization in FePc and CoPc, while adding one electron to ligand π orbitals in NiPc and CuPc. This has opposite consequences on the molecular magnetic moment: In FePc and CoPc the interaction with the substrate tends to reduce the TM spin, whereas, in NiPc and CuPc, an additional spin is induced on the aromatic Pc ligand, leaving the TM spin unperturbed. In CuPc, the presence of both TM and ligand spins leads to a triplet ground state arising from intramolecular exchange coupling between *d* and π electrons. In FePc and CoPc the magnetic moment of C and N atoms is antiparallel to that of the TM. The different character and symmetry of the frontier orbitals in the TMPc series leads to varying degrees of hybridization and correlation effects, ranging from the mixed-valence (FePc, CoPc) to the Kondo regime (NiPc, CuPc). Coherent coupling between Kondo and inelastic excitations induces finite-bias Kondo resonances involving vibrational transitions in both NiPc and CuPc and triplet-singlet transitions in CuPc.

DOI: 10.1103/PhysRevB.85.155437 PACS number(s): 75.70.−i, 75.20.Hr, 75.50.Xx, 68.37.Ef

I. INTRODUCTION

The interaction of molecules with solid surfaces governs the self-assembly of supramolecular layers[1,2] as well as the electronic and magnetic properties of metal-organic heterostructures[2,3] and single-molecule devices.[4,5] The large variety of organic and metal-organic complexes, combined with the possibility of tuning the chemical reactivity and electronic ground state of different complexes within the same family of molecules, make such systems increasingly attractive for applications. However, electronic interactions at the interface with a metal may induce charge transfer, distort the ligand field, and reduce electron-electron correlation effects via screening and hybridization. The intricate interplay between all these processes is far from being understood.

Transition-metal phthalocyanines (TMPc) represent a well-known class of molecules with organic semiconducting properties in the bulk and a broad spectrum of applications that includes field-effect transistors, gas sensors, and photovoltaic cells.[6] Due to their relatively simple and robust structure as well as versatile chemistry, TMPc have assumed the role of a model system to study the interaction of metal-organic complexes with metal surfaces. Their flat adsorption geometry facilitates the bonding of both the central TM ion and organic ligands to the substrate, whereas their capability to coordinate many different metal atoms allows for a systematic investigation of their magnetic properties.

The interaction of TMPc with metal surfaces has been studied by many techniques, including scanning tunneling microscopy (STM),[2,7–25] ultraviolet and x-ray photoelectron spectroscopy (UPS-XPS),[9,26–29] x-ray absorption spectroscopy (XAS),[3,9,30–32] and density functional theory (DFT).[33–36] Investigations of the magnetic properties of TMPc have mostly focused on MnPc,[24,36] FePc,[3,14,15,36] and CoPc,[3,19–23,34–36] for which it was shown that adsorption on a metallic surface tends to quench the magnetic moment of the TM ion. A corollary to such investigations is the implicit assumption that the magnetic properties of TMPc at surfaces depend almost exclusively on the ground state of the TM ion. However, a recent investigation by our group has highlighted the possibility of inducing a magnetic moment delocalized over the Pc organic ligand, which affects the spin degeneracy and symmetry of the molecular ground state as well as the electrical conductance measured at different sites within the same molecule.[7] Unpaired spins induced by charge transfer in Pc ligands have also been found to affect the conductance properties of $TbPc_2$ single-molecule magnets adsorbed on Au[37] and their coupling to ferromagnetic surfaces.[38] Indeed, a growing number of experiments indicates that the organic ligand directly affects the magnetism and transport properties of metal-organic[23,39,40] as well as purely organic complexes[41] adsorbed on surfaces.

These results evidence the need to take into account the full molecular structure in order to understand and predict the magnetic properties of adsorbed systems. Here we present a comprehensive study of four different TMPc (TM = Fe, Co, Ni, Cu) deposited on Ag(100) in order to shed light on the mechanisms that lead to changes of both the TM and ligand magnetic moments at the TMPc/metal interface. Scanning

tunneling spectroscopy (STS) combined with DFT allows us to elucidate the role of charge transfer, hybridization, and correlation at the molecule-metal interface on the magnetic properties. The paper is organized as follows: after presenting the experimental and theoretical methods (Sec. II), we first introduce the theoretical electronic structure of TMPc in the gas phase (Sec. III), which serves as the starting point of our investigation. We then describe the experimental and theoretical adsorption geometry of the molecules on Ag(100) (Sec. IV), including a discussion of electronic chirality effects, which were revealed in a previous work on CuPc.[2] The electronic structure of adsorbed TMPc is discussed in Sec. V, where STS data are compared with the molecular projected density of states (PDOS) derived from *ab initio* DFT calculations. The magnetic properties of TMPc are addressed in Sec. VI using STS to measure the intensity and spatial extension of Kondo anomalies in the differential conductance, including the coupling to vibrational and magnetic degrees of freedom in NiPc and CuPc as well as the theoretical description of triplet-singlet excitations in CuPc using a multiorbital approach. Further, we calculate the magnetic moments of adsorbed TMPc and compare them to the gas-phase magnetic moments in neutral and negatively charged species in order to understand the effects of charge transfer and intramolecular exchange and their dependence on the TM ion. Finally, Sec. VII summarizes the more general conclusions of this work.

II. METHODS

A. Experiment

TMPc were evaporated in ultra high vacuum (UHV) from a heated alumina crucible onto a sputter-annealed Ag(100) single crystal kept at room temperature, after degassing the 99% pure powder material (Sigma Aldrich) for 24 h. The deposition rate was ∼0.05 monolayers per minute; the base pressure during evaporation was below 5×10^{-10} mbar. Spectroscopic measurements were performed using an STM operating at 5 K. Conductance (dI/dV) spectra were obtained with the lock-in technique, using a bias voltage modulation of frequency 3 kHz and amplitude 1 mV_{rms} for the low-energy spectra ($-0.1 < V < 0.1$ V), and 3 mV_{rms} for the larger energy range ($-2 < V < 1$ V). A background spectrum acquired on the bare Ag surface with the same feedback conditions was subtracted to all spectra in order to enhance molecular resonances and minimize features originating from the tip or substrate electronic structure.[42] Hence, only relative dI/dV values are significant in these spectra. dI/dV maps were acquired in the constant current mode, with an amplitude of 10 mV_{rms}. Maps of the Kondo resonance were obtained using the d^2I/dV^2 signal in order to scan at a finite voltage, with a modulation amplitude of 3 mV_{rms}.[7] Both topographic and conductance images were processed using the WSxM software.[43] Further details on the spectroscopic methods can be found in the Supplementary Information of Ref. 7.

B. Theory

The theoretical electronic structure of both gas-phase and adsorbed TMPc have been obtained from *ab initio* calculations using the VASP implementation of DFT in the projected augmented plane-wave scheme.[44,45] Different approximations, namely local-density approximation (LDA),[46] generalized gradient approximation (GGA),[47] GGA+van der Waals (vdW),[48,49] and GGA+U,[50] have been compared in order to obtain consistent results and to check the effect of different exchange-correlation approximations or the vdW interaction. Unless otherwise stated, the results presented in the next sections were obtained using GGA + U[50] and vdW corrections using the scheme of Grimme;[48,49] $U_{\text{eff}} = U - J$ was chosen to be 3 eV in all cases. Additional tests were made to check that reasonable values of U_{eff} do not qualitative change our conclusions. The plane-wave cutoff energy was set to 300 eV. The calculated slab included five Ag atomic layers intercalated by seven vacuum layers in the vertical direction and a 7×7 lateral supercell. The positions of all atoms in the molecule and the first three Ag layers were relaxed vertically and laterally until forces were smaller than 0.05 eV/Å. The projected density of states (PDOS) of NiPc have been used to compare single ($1 \times 1 \times 1$) and multiple ($5 \times 5 \times 1$) k-point calculations, which converge after applying a broadening of 100 meV to the data. Based on that, the results for a single k point with the latter broadening are used in the following. Charge transfer and local magnetic moments have been calculated using a Bader charge analysis.[51,52]

III. GAS-PHASE TMPc

Before discussing the effects of adsorption on the molecular electronic and magnetic structure, we briefly introduce the chemical configuration of gas-phase TMPc, as well as the electronic structure obtained from spin-polarized calculations, which will be used later as a reference.

TMPc are characterized by a rather simple and stable molecular structure, where the TM ion bonds to four isoindole (pyrrole+benzene) ligands via their pyrrole N (N_p). That leaves the ion in a $[TM]^{2+}$ state, and the molecule with the square planar D_{4h} symmetry. Under this symmetry group, the d states transform as b_{2g} (d_{xy}), b_{1g} ($d_{x^2-y^2}$), a_{1g} (d_{z^2}), and e_g (d_{xz}, $d_{yz} = d_\pi$). Depending on their symmetry and energy position, these orbitals mix to a different degree with $2p$ states of the C and N atoms. The highest occupied and lowest unoccupied molecular orbitals (HOMO and LUMO) of the Pc ring are represented by delocalized a_{1u} and $2e_g$ π orbitals, respectively, with marginal contribution from the TM d states. The TM-related MO can be classified into two groups according to their parallel (b_{2g}, $b_{1g} = d_\parallel$) or perpendicular (a_{1g}, $e_g = d_\perp$) orientation with respect to the molecular plane, and, hence, the substrate.

Figure 1 shows the spin-up and spin-down energy levels of TMPc near the frontier orbitals obtained within the GGA + U scheme. The $3d$ contribution in each MO is indicated between parentheses; the molecular magnetic moments are discussed in Sec. VI. Our calculations show that the electronic structure of the Pc ring is barely affected by the TM ion. This is clearly seen in the a_{1u} and $2e_g$ ligand orbitals: The a_{1u} MO, with negligible d contribution, appears at the same energy in all molecules. The $2e_g$ energy varies slightly with the d configuration of the TM ion as this orbital exhibits a finite d_π contribution that ranges from 7% in FePc to 1% in CuPc.

The evolution of the electronic configuration of the central $[TM]^{2+}$ ions cannot be rationalized by the simple filling of

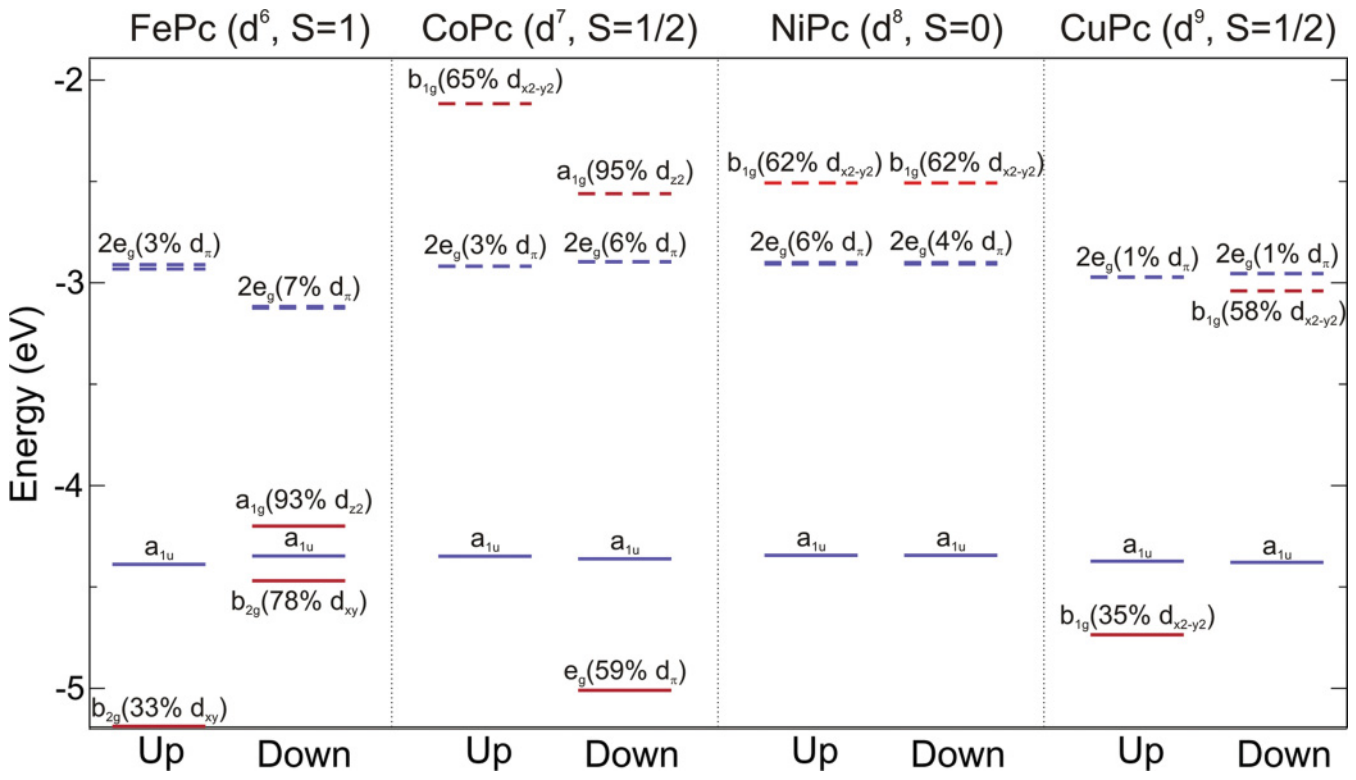

FIG. 1. (Color online) Spin-polarized electronic structure of gas-phase TMPc. (Un-) occupied states are represented by (dashed) full lines. The contribution of different d states is indicated in percentage.

one-electron energy levels split by the ligand field, due to the strong d-d correlation and the energy-dependent hybridization with ligand states. The situation is most critical for the ground state of FePc, where the quasidegeneracy between different electronic terms[3,53] has led to a long-standing debate in literature.[54–59] The discussion of such differences is beyond the scope of this paper. However, the spin moment that we obtain for this molecule is $S = 1$, independently of the DFT functional and in good agreement with previous work.[3,53–59] CoPc, with one electron more, presents a robust $^2A_{1g}$ ($S = 1/2$) ground state with a single a_{1g} (d_{z^2}) hole, in agreement with x-ray absorption measurements.[3] NiPc, with d^8, has a singlet ($S = 0$) $^1A_{1g}$ ground state. The TM spin is recovered in CuPc, with a single hole in b_{1g} ($d_{x^2-y^2}$), resulting in a doublet ($S = 1/2$) $^2B_{1g}$ ground state.

IV. ADSORPTION OF TMPc ON Ag(100)

A. Adsorption geometry

The adsorption of individual TMPc has been studied by STM. Their topographic appearance already reflects differences that allow us to classify them into two groups: The TM ion appears as a protrusion in FePc and CoPc and a depression in NiPc and CuPc, as shown in Figs. 2(a) and 3. The different contrast is due to the large (small) coupling of the TM $d_\perp$ ($d_\parallel$) orbitals near the Fermi level (E_F) with the tip states.[60] As typical for TMPc on metals, the molecules adsorb with the aromatic plane parallel to the surface. Atomically resolved images of the surface reveal two different azimuthal orientations of the TM-N_p ligand axis [Fig. 2(b)], corresponding to $\pm 30^\circ$ with respect to the [011] surface direction. Previous systematic *ab initio* calculations of CuPc on Ag(100) revealed that this orientation, with the TM ion located on the Ag hollow site, corresponds to the minimum of the adsorption energy.[2] A similar adsorption site has been found for CuPc on Cu(100) (Ref. 61). The rotation of the Pc macrocycle with respect to the substrate high-symmetry

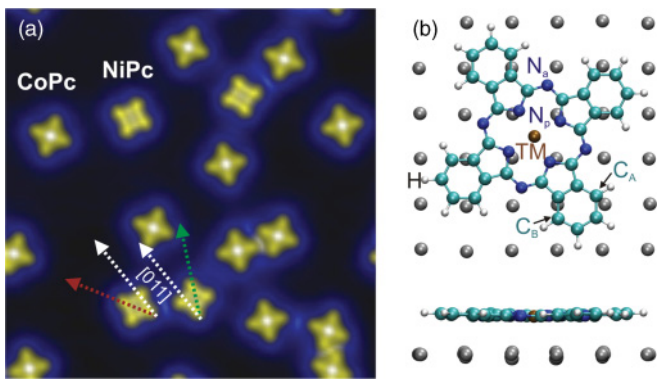

FIG. 2. (Color online) (a) Topographic image of CoPc and NiPc molecules codeposited at room temperature on the Ag(100) surface ($I = 0.49$ nA, $V = -1.0$ V), image size 13.4×13.4 nm^2. The green/red arrow indicates the $+/-30^\circ$ rotation of the molecular axis with respect to the surface lattice vectors (white arrows). (b) Adsorption geometry of NiPc on Ag(100) calculated by DFT. The different elements are labeled. N_a and N_p refers to aza and pyrrole N, and C_A and C_B to the two C atoms of the benzene ring used to measure chiral distortions (Table I).

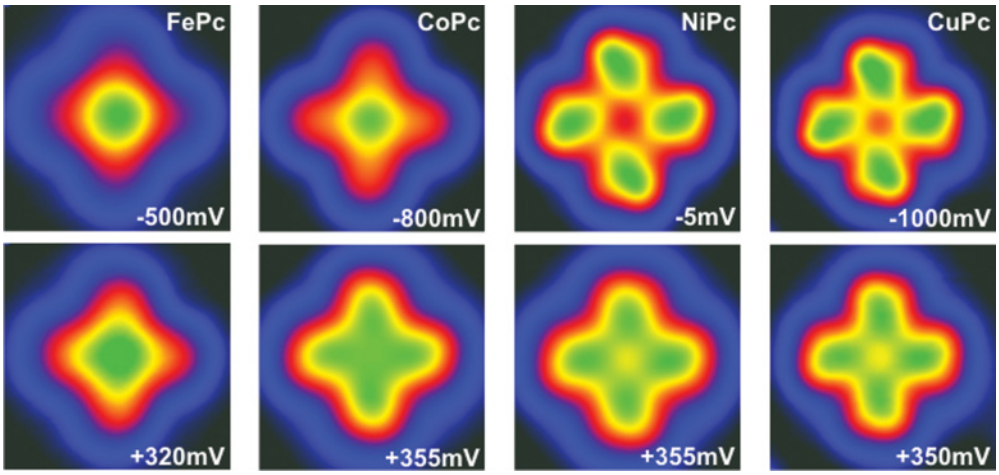

FIG. 3. (Color online) Bias-dependent topographic images of all TMPc. For CuPc and NiPc negative voltage images with maximum chiral contrast are displayed. The contrast of CoPc and FePc does not vary in the range of negative voltages investigated. For positive voltage, all TMPc appear achiral in the bias range $V < +1$ V.

directions was attributed to bond optimization between aza-N (N_a) and Ag atoms. This study confirms the leading role of the N_a-Ag interaction, as both theory and experiment find very similar adsorption configurations for all TMPc, independently of the central TM ion [see Fig. 2(b)].

The calculations also show that TMPc become slightly concave after deposition, with the periphery of the molecule slightly further from the surface. This effect is most pronounced in the case of FePc. The molecules also induce a small distortion of the substrate, pushing the Ag atoms below N_p slightly below the surface plane and the Ag atoms below N_a slightly above it. The molecule-substrate distances, calculated as the difference in the z coordinate between the TM atom and the Ag atom below N_p, are shown in Table I. The distance obtained with LDA is ∼2.5 Å for the four molecules. This method is known to overbind, compensating for the absence of vdW forces. These forces are included in the GGA + vdW method. The results with GGA + vdW show that z increases to ∼2.7 Å, keeping it TM independent. Similar values were also found using both methods for CoPc adsorbed on Cu(111) (Ref. 34). On the less-reactive Au(111) surface, however, distances obtained with LDA for different TMPc do not level out and still reflect a TM-dependent behavior.[33,36] In our case, we can separate the effect of the interaction between the TM ion and the substrate by using plain GGA, i.e., by switching off the vdW interaction. Using this method, we find that FePc and CoPc, with $z = 2.76$ and 3.08 Å, respectively, are significantly closer to the surface than NiPc and CuPc, with $z = 3.59$ and 3.47 Å, respectively. The stronger TM-Ag interaction of FePc and CoPc is attributed to the direct participation of the d orbitals to the molecule-substrate bonds.[26,33,36] The vdW interaction introduced by GGA + vdW can be estimated by the correction added to the total energy calculated by GGA alone. This correction is larger by about 1 eV for NiPc and CuPc compared to FePc, which compensates for the lack of direct TM-substrate interaction in the former species and results in the nearly TM-independent bond length reported in Table I.

TABLE I. Computed height distances z (in Å) between the TM ion and the Ag atom below N_p, obtained within different DFT approximations, and height difference between C_A and C_B atoms at the end of the benzene ring [see Fig. 2(b)] obtained with GGA + vdW.

	GGA	GGA + vdW	LDA	$z(C_A\text{-}C_B)$
FePc	2.76	2.64	2.43	0.04
CoPc	3.08	2.72	2.49	0.01
NiPc	3.59	2.74	2.53	0.02
CuPc	3.47	2.79	2.46	0.02

B. Electronic chirality

Figure 3 shows that NiPc and CuPc present chiral contrast at negative bias, whereas FePc and CoPc appear achiral at both negative and positive bias. This effect has been studied in detail for CuPc/Ag(100) in Ref. 2, where it has been shown that the chiral contrast observed by STM is not related to nuclear distortions but originates from the asymmetric electronic interaction between the a_{1u} and $2e_g$ orbitals and Ag states. This asymmetry is due to the misalignment between surface and molecular symmetry axes, where the $+30°$ and $-30°$ configurations imprint chiral charge distortion of opposite sign. Here we extend this study to FePc, CoPc, and NiPc and quantify the contribution of conformal distortions to the chiral contrast. We use the height difference between two opposite C atoms at the benzene ring as a measure of their torsion [see Table I and Fig. 2(b)]. Its small value, close to the calculation's accuracy, obtained for all TMPc, confirms the electronic origin of chirality. This is in line with the voltage dependence of the chiral contrast and the fact that it is observed only in CuPc and NiPc in spite of the similar geometry found for all molecules.

Electronic chirality is imprinted to each MO to a different degree, depending on their spatial distribution and hybridization with the substrate, with maximum effect in orbitals exhibiting a nodal plane on the TM-N_p ligand axis (see Fig. 5). The a_{1u} MO exhibits the strongest distortion because of its double lobe structure at the benzene ring, where the asymmetry of charge distortion is maximum. The chiral contrast at the $2e_g$ MO, also with nodal planes on the ligand axis, varies with

energy: At positive bias it is strongly reduced but becomes more intense when shifted to negative bias due to charge transfer. The MOs with significant TM-d contribution do not have nodal planes on the ligand axis and, hence, do not present any significant chirality. This leads to a voltage-dependent chiral appearance of the TMPc that depends solely on the specific electronic structure of each molecule, as shown in Fig. 3. CuPc and NiPc are strongly chiral at negative bias due to the asymmetry of the a_{1u} orbital and of the partially occupied $2e_g$ orbital, and achiral at positive bias, where tunneling occurs via a more symmetric $2e_g$ resonance. In CoPc and FePc, on the other hand, the $2e_g$ orbital only appears at positive bias, where the chiral contrast is insignificant. Furthermore, TM-d states and other other interface-related resonances with maximum intensity on the ligand axis hinder the chirality of the a_{1u} state.

V. ELECTRONIC STRUCTURE

In this section, we present scanning tunneling spectroscopy (STS) measurements of the molecules adsorbed on the Ag(100) surface. The energy of the MOs and other interface-related features is obtained from individual dI/dV spectra, whereas maps of the dI/dV intensity at specific energies reveals their symmetry and spatial distribution within the molecule. Experimental results are then compared to the theoretical density of states projected onto different MOs, which allows us to assign the observed dI/dV peaks to specific orbitals, providing insight into the formation of hybridized molecule-substrate states, charge transfer, and molecular magnetism.

A. Scanning tunneling spectroscopy

Figure 4(a) shows the dI/dV spectra of FePc to CuPc recorded by positioning the STM tip on the central TM atom (red curves) and on a peripheral benzene ring (blue curves). The a_{1u} and $2e_g$ resonances corresponding to the HOMO and LUMO of the gas-phase Pc ring can be easily identified by studying the spatial distribution of the dI/dV peaks of the spectra acquired on benzene, as shown in Fig. 5. The intensity distribution of these resonances is similar to that found for other substrates,[20] except for the chiral fingerprint discussed in the previous section. The energy position of the a_{1u} state is similar in all TMPc, varying continuously from -1.14 V in CoPc to -1.40 V in CuPc (FePc was not measured in this energy range). On the other hand, the spectral distribution of the $2e_g$ state critically depends on the TM ion: In FePc and CoPc, a single unoccupied peak is observed at $+0.47$ and $+0.39$ V, respectively, as expected for the Pc LUMO. Conversely, CuPc and NiPc exhibit two peaks around the Fermi level, located at $-0.29/+0.35$ V and $-0.35/+0.35$ V,

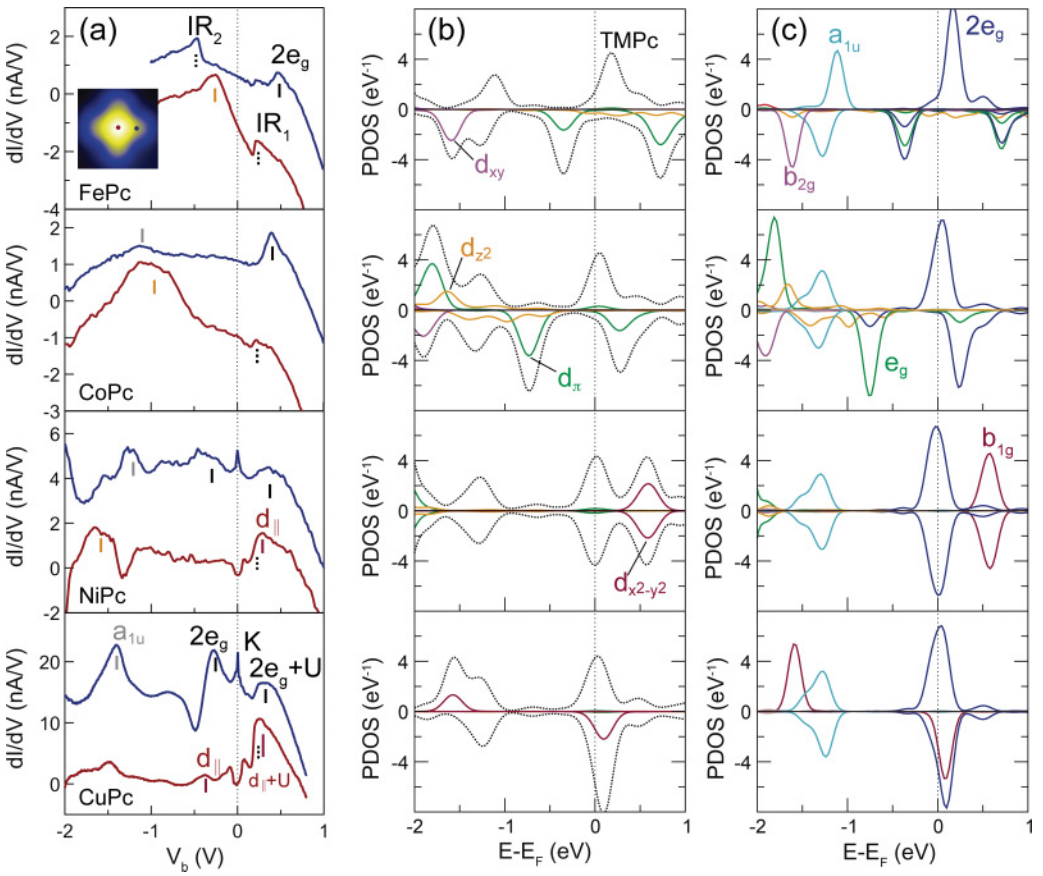

FIG. 4. (Color online) (a) dI/dV spectra, acquired on the TM ions (red, bottom) and benzene rings (blue, top). The latter spectra have been offset for clarity. MOs, interface (IR), and Kondo (K) resonances are labeled. The weak Kondo peak at the ion site is smeared out by the larger V_{mod} used as compared to Fig. 7. Tunneling conditions (I, V): 1 nA, -1.0 V (FePc, CoPc), 3 nA, -2.2 V (NiPc), 3 nA, -2.0 V (CuPc). (b) Computed spin-polarized DOS of TMPc (black), and its projection onto the TM d states. (c) Computed spin-polarized PDOS projected onto MOs.

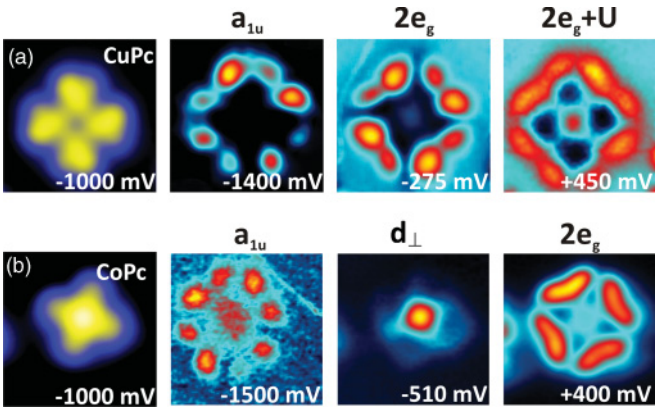

FIG. 5. (Color online) Constant current dI/dV maps of (a) CuPc and (b) CoPc. A topographic image of each molecule recorded simultaneously during the acquisition of the maps is displayed on the left side. The color scale is adjusted for maximum contrast in each map. NiPc and FePc present similar MO distributions as CuPc and CoPc, respectively.

respectively. Both peaks, however, can be associated with the $2e_g$ state due to their similar spatial distribution. The position of the lowest energy peak below E_F indicates that this orbital is partially occupied. The energy splitting of ~0.65–0.70 eV is within the range of the Coulomb repulsion energies obtained for π orbitals in aromatic complexes of similar size.[41,62,63] We, therefore, assign the peaks at negative and positive bias to single and double occupation of the $2e_g$ state, respectively, in agreement with the results reported in Ref. 7. The sharp peak appearing between the two $2e_g$ "Coulomb blockade" peaks is the Kondo resonance associated to the unpaired ligand spin,[7] which will be discussed further in Sec. VI. Note that the short electron lifetime of empty orbitals in molecules coupled to metals prevents their double occupation by tunneling electrons, which would lead to similar "Coulomb blockade" peaks in the $2e_g$ state of FePc and CoPc.

Spectra recorded on the TM ions, shown as red curves in Fig. 4(a), allow us to identify the MOs with d character. The broad peak shifting downward with increasing d occupation from FePc to NiPc can be related to $d_\perp$ states, easiest to observe due to their effective coupling with the STM tip. In CuPc, these states are situated below the probed energy range. The localization of this peak on the TM ion is confirmed by the dI/dV map of CoPc at −510 mV [Fig. 5(b)]. In this molecule, the $d_\perp$ resonance appears well below E_F, suggesting the complete filling of the a_{1g} (d_{z^2}) orbital and, hence, a switch in the charge transfer channel from the ligand $2e_g$ to TM-d states compared to NiPc and CuPc. In FePc, the tail of the $d_\perp$ peak crosses E_F, suggesting that these states are not fully occupied, similarly to FePc on Au(111) (Ref. 3).

Contrary to the $d_\perp$ states, the perturbation of the $d_\parallel$ states due to adsorption appears to be minor. Although confinement in the molecular plane makes them difficult to access by STS, some features in the spectra of NiPc and CuPc can be tentatively assigned to the b_{1g} ($d_{x^2-y^2}$) state. In the pristine molecules, this orbital is singly occupied in CuPc and unoccupied in NiPc (see Fig. 1). The intensity corresponding to the unoccupied b_{1g} state is masked by a steplike interface resonance feature (IR_1) that we observe around +0.2 V in

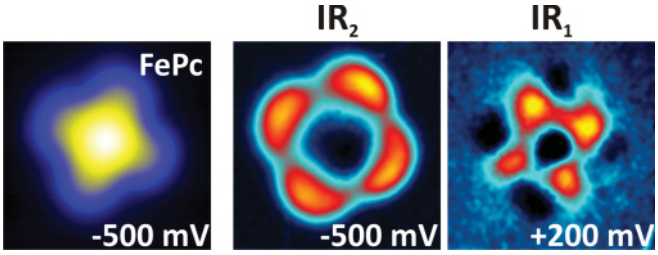

FIG. 6. (Color online) Constant current dI/dV maps of interfacial resonances in FePc arising from the hybridization between molecular and substrate electrons, marked as IR in Fig. 4(b). The topography of FePc recorded during the acquisition of the maps is displayed on the left side.

all molecules. However, both CuPc and NiPc exhibit a larger dI/dV signal in this energy range compared to CoPc and FePc, which suggests that there is an additional orbital contributing to the tunneling current above E_F. The singly occupied b_{1g} state in CuPc can be assigned to the small hump observed around −0.4 V, close to where the $2e_g$ resonance on the benzene spectra presents a pronounced valley. This valley, absent in NiPc at this energy, is tentatively assigned to a Fano resonance originating from the tunneling interference between the occupied b_{1g} and the more hybridized $2e_g$ states, analogous to that occurring between resonant and direct channels in impurity and quantum dot systems.[64–66] Indeed, the dip observed in NiPc at −1.4 V, where $d_\perp$ states overlap with the a_{1u} orbital, might have a similar origin, supporting the presence of Fano peaks in these molecules.

In addition to MO resonances that maintain the original character of the TMPc states, we find additional interface resonances that originate from strong hybridization with Ag electrons (see Fig. 6). The IR_1 resonance observed at +0.2 V [Fig. 4(a)] is common to all TMPc and only observed on Ag(100). This resonance could originate from the hybridization of molecular states with the lowest-lying unoccupied surface state of Ag(100), which is close in energy.[67] In FePc, we observe an additional feature (IR_2) between the a_{1u} and $d_\perp$ states, which we identify with an interface state with intensity at the benzene rings, similarly to that reported for CoPc on Au(111) (Ref. 20).

B. Density of states calculated by DFT

In order to correlate the features observed in the dI/dV spectra with the molecular electronic structure, we have computed the PDOS projected onto the TM-d states as well as on the MOs of the TMPc, as shown in Fig. 4. In general, we find fair agreement between the measured and calculated resonances, supporting the assignment of the spectral features to specific MO based on the symmetry and spatial distribution of the dI/dV intensity.

The strongest hybridized states are the a_{1g} MOs of FePc and CoPc, as expected due to their dominant d_{z^2} character. The TM d_{z^2} electrons hybridize with the Ag-sp_z states, confirming the strong, direct substrate-TM interaction discussed in Sec. IV. Additionally, in the case of FePc and CoPc, two $2e_g$ and one e_g state are mixed together, projecting onto one occupied and one empty spin-down resonances [see Fig. 4(c)]. Mixing is induced by hybridization with the substrate, showing that the picture

TABLE II. Computed charge transfer ΔN (in electrons) for the adsorbed molecules and total magnetic moment m (units of μ_B) in neutral and anionic gas-phase and adsorbed molecules.

	ΔN	$m^{\text{gas}}_{\text{TMPc}}$	$m^{\text{gas}}_{[\text{TMPc}]^{1-}}$	$m^{\text{ads}}_{\text{TMPc}}$
FePc	0.80	2.00	1.00	1.06
CoPc	0.99	1.00	0.00	0.63
NiPc	1.13	0.00	1.00	0.14
CuPc	0.81	1.00	2.00	1.32

of slightly distorted MO is no longer valid in this case. This is in line with the appearance of interface resonance as those observed in STS maps (IR_2 in Fig. 6). For NiPc and CuPc, hybridization with the substrate turns out to be much smaller, and the PDOS resembles that of the gas-phase molecules of Fig. 1. In these two cases the confinement of the b_{1g} orbital in the molecular plane and its σ character reduces hybridization with Ag electrons, diminishing the charge transfer to this orbital. Hence, it appears unoccupied in NiPc and singly occupied in CuPc, as in the gas phase.

The a_{1u} orbital, fixed at about -1.30 eV, is the only MO that is not affected by the d occupation of the TM ion. In the case of FePc, the spin-up and spin-down a_{1u} states are exchange split due to the single-configurational nature of DFT. This broken symmetry reflects the strong spin polarization of the whole molecule. The position of the $2e_g$ MO, on the other hand, depends strongly on the type of TM ion and reveals a transition in the interaction with the substrate. As in the dI/dV spectra, the PDOS shows that this state is unoccupied in FePc, partially occupied in CoPc, and acquires a charge of approximately one electron in NiPc and CuPc. The splitting between occupied and unoccupied $2e_g$ states is not fully reproduced in the calculations due to the well-known electronic gap problem in DFT, which is especially critical for delocalized π orbitals.[68]

The origin of the charge-transfer behavior with TM can be unfolded by using gas-phase anions to study pure transfer without hybridization. We find that the TM-d dependent behavior is the same as in adsorbates. In $[\text{FePc}]^{1-}$ and $[\text{CoPc}]^{1-}$ the effect of the extra electron is complex and the extra charge is not easily assigned to a single MO. It, rather, induces a reorganization of the charge within the molecule. In $[\text{NiPc}]^{1-}$ and $[\text{CuPc}]^{1-}$ the behavior is simpler, with the extra electron going to $2e_g$. The observed behavior is also in agreement with transport results in electron-doped thin films.[69]

In summary, although the net amount of transferred charge is about one electron in all cases (see Table II), its effect on the molecule depends on the d occupation of the ion. This difference is driven by the interplay between energy alignment and Coulomb repulsion in the d and $2e_g$ states, as well as their degree of hybridization with the substrate. The similarity between results obtained by calculating gas-phase anions and adsorbates indicates that the leading role of the substrate is that of a charge reservoir.

VI. MAGNETIC PROPERTIES

The magnetic properties of TMPc on Ag(100) are addressed using STS through the analysis of dI/dV spectra close to E_F. The presence of sharp zero bias resonances can be used to detect the formation of local magnetic moments screened by the Kondo effect.[70,71] This occurs as itinerant electrons belonging to the substrate couple antiferromagnetically to a localized spin, forming a many-body singlet state at temperatures below the characteristic Kondo energy $k_B T_K$. dI/dV maps of the Kondo spectral features further allow us to measure the spatial distribution of the spin density for unpaired electrons. We note, however, that, although the presence of a Kondo resonance is a signature of a local moment, its absence is not a proof of a nonmagnetic ground state, since the resonance can also be experimentally inaccessible due to the low T_K in weakly interacting spins. In such a case, STS data have to be contrasted with complementary experiments, such as x-ray magnetic circular dichroism[3,32] or, as in the present case, with theoretical calculations.

A. Kondo effect probed by STS

Figure 7 shows the dI/dV spectra measured near E_F for the four molecules at the position of the TM ion (red curves) and benzene ligand (blue curves). FePc and CoPc present featureless spectra, which indicate that the Kondo interaction between these molecules and the Ag(100) surface is either absent or too weak to be observed at 5 K. Relatively flat Co spectra were reported also for CoPc adsorbed on Au(111), for which it was concluded that the filling of the a_{1g} state leads to a complete quenching of the molecular magnetic moment.[19] This interpretation has been recently questioned based on a mixed-valence model of x-ray absorption spectra.[3] In both cases, the quenching of the CoPc magnetic moment appears to be a robust result. On the other hand, FePc does present a Kondo resonance on Au(111), although different interaction strengths have been reported.[14,16] We attribute the absence of Kondo peaks on Ag(100) to a stronger interaction with the substrate, as reflected by the substantial hybridization of the $d_\perp$ states, which may lead to a mixed-valence configuration of FePc, as discussed later.

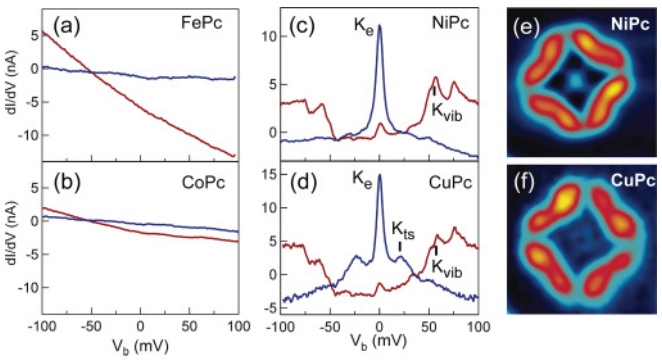

FIG. 7. (Color online) [(a)–(d)] Conductance spectra acquired around E_F on the TM ions (red) and benzene rings (blue). The zero-bias (elastic), vibrational, and triplet-singlet Kondo resonances observed in CuPc and NiPc are labeled as K_e, K_v, and K_{ts}, respectively. Tunneling conditions (I, V_b): 1 nA, -100 mV (FePc, CoPc), 1.1 nA, -100 mV (NiPc), 2 nA, -100 mV (CuPc). [(e) and (f)] d^2I/dV^2 maps acquired at -3 and -5 mV, respectively, showing the intensity distribution of the elastic Kondo resonance (K_e) of CuPc and NiPc and its close resemblance to the $2e_g$ resonances.

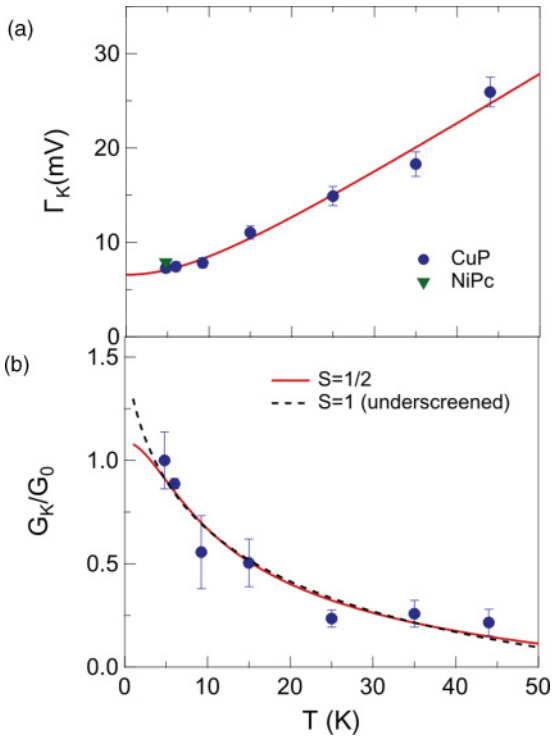

FIG. 8. (Color online) Temperature dependence of (a) Γ_K and (b) G_K normalized to the intensity at 5 K (G_0) of the elastic Kondo resonance of CuPc. The solid line in (a) is a fit of Γ_K using Eq. (1) giving $T_K = 27 \pm 2$ K. The solid (dashed) line in (b) is a fit of G_K/G_0 for the $S = 1/2$ (underscreened $S = 1$) case of Eq. (2).

In contrast with FePc and CoPc, NiPc and CuPc present many characteristic signatures of low-energy excitations around E_F. Such excitations have been discussed in detail in Ref. 7. Here we report a summary of these results for comparison with theory as well as to provide a complete picture of TMPc adsorbed on Ag(100). The most prominent feature of the NiPc and CuPc spectra is the presence of an intense zero bias resonance with maximum intensity at the ligand position. This is rather unusual for metal-organic adsorbates since, in most cases, Kondo resonances are associated to the spin of the TM ions.[14,16,19,24,25] Here, the zero bias peak is assigned to an elastic Kondo resonance (K_e) arising from the unpaired spin located in the $2e_g$ orbital of CuPc and NiPc. Note that the finite value of the resonance at the ion site is related to the nonvanishing intensity of $2e_g$ at this site, as can be seen in the spin density distribution of the NiPc anion in Fig. 10. The assignment of the zero-bias resonance to the Kondo effect is supported by the temperature dependence of the peak's full width at half maximum (Γ_K) and maximum intensity (G_K). Figure 8 shows that both parameters follow expressions derived from Fermi liquid theory[72] and numerical renormalization group (NRG):[73,74]

$$\Gamma_K(T) = 2\sqrt{(\pi k_B T)^2 + 2(k_B T_K)^2}, \quad (1)$$

$$G_K(T) = G_{\text{off}} + G(0)\left[1 + \left(\frac{T}{T_K}\right)^{\xi}(2^{1/\alpha} - 1)\right]^{-\alpha}. \quad (2)$$

where α and ξ are parameters that depend on the total spin of the molecule. Fitting the values of Γ_K with Eq. (1) leads to a Kondo temperature of $T_K = 27 \pm 2$ K for CuPc. The logarithmic behavior of G_K makes it more sensitive to the scattering of the data, but we find that expressions for both $S = 1/2$ and (the underscreened) $S = 1$ fit reasonably well the data by using $T_K = 27$ K. The two possible spin states will be discussed later.

We notice that NiPc and CuPc present very similar Kondo resonances in spite of the $S = 0$ ground state of the Ni ion and $S = 1/2$ ground state of Cu. Indeed, we estimate a Kondo temperature $T_K = 29$ K for NiPc from Γ_K measured at 5 K. Moreover, the intensity of both CuPc and NiPc resonances closely follows the contour of the $2e_g$ orbital, as revealed by the remarkable similarity of the dI/dV maps reported in Figs. 7(e) and 7(f) compared to Fig. 5. These observations indicate the presence of an unpaired spin localized on the $2e_g$ ligand state, in agreement with the single occupancy of this orbital discussed in Sec. V. The relation among energy, width, and Coulomb repulsion potential, with values of $\epsilon = -0.30$ eV, $\Gamma \sim 0.30$ eV, and $U = 0.65$ eV, respectively, is also characteristic of the Kondo regime, for which $|\epsilon|, |\epsilon + U| \geqslant \Gamma$.

The direct observation of the "Coulomb blockade" peaks and the Kondo resonance allows, unlike in previous studies of molecular adsorbates, for a univocal identification of the MO associated to the unpaired spin. As the spin participating to the many-body Kondo state originates from a single orbital, we expect a well-defined value of T_K over the whole molecule, as confirmed by our observations. This is in contrast with the variations of T_K found for Co porphyrins adsorbed on Cu(111), which suggest a spatially dependent, multiple orbital origin of the Kondo interaction, possibly due to strong intermixing of TM and ligand orbitals near E_F (Ref. 40).

B. Inelastic vibrational and Kondo excitations

The dI/dV spectra of NiPc and CuPc recorded on the TM ions [red curves in Figs. 7(c) and 7(d)] present a complex series of peaks and conductance steps in addition to the elastic Kondo resonance observed at zero bias. It is well known that inelastic excitations induce steplike increases in the differential conductance spectra symmetrically distributed in energy around E_F.[75,76] In Kondo systems, the coherent coupling of the Kondo state with such excitations leads to additional peaks at the energies of the inelastic conductance steps.[77] Unlike quantum dots, where the reduced orbital level-spacing favors the coupling of Kondo and electronic excitations,[78] the origin of such side peaks in small aromatic molecules is restrained to vibrational[41,79–81] (K_v) or magnetic[39,73,82–84] (K_{ts}) excitations. In the present case, by comparing the energy of the K_v peaks with that of the Raman vibrational modes of gas-phase CuPc,[85] we find that the inelastic features found at the position of the Ni and Cu ions [Fig. 9(a)] correspond to vibrational excitations that involve distortion of the TM-N_p bonds.[7] Note that the vibrational spectra of NiPc and CuPc are nearly identical, as shown by the twin d^2I/dV^2 spectra displayed in the bottom graph. The steplike and peaklike contributions to the inelastic conductance can be obtained by fitting the dI/dV spectra with step and Lorentzian functions, as shown in Fig. 9(a). From the fit of the spectra we observe that both NiPc and

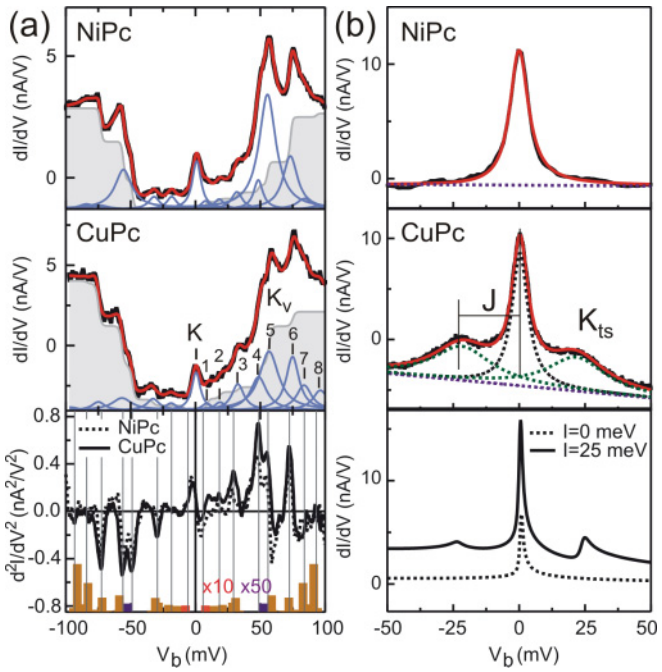

FIG. 9. (Color online) Fit of the differential conductance (dI/dV) spectra of NiPc and CuPc measured at (a) the position of the TM ion and (b) the benzene ring, using Fano and Lorentzian functions for the zero and finite bias peaks, respectively, and step functions for the inelastic conductance steps. The bottom graph in (a) shows the second derivative (d^2I/dV^2) of the spectra measured on Ni and Cu. The energies obtained from the fits are indicated by dashed lines in the d^2I/dV^2 spectra. The bars correspond to the intensity of calculated Raman (yellow) and infrared (gray) modes of gas phase CuPc.[85] The bottom graph in (b) shows the theoretical PDOS obtained for the $2e_g$ orbital of CuPc for $I = 25$ meV (solid line) and 0 meV (dashed line) calculated within the noncrossing approximation (see text for details).

CuPc present more intense conductance steps at negative bias and more intense Kondo peaks at positive bias. These inverted correlation between vibrational and Kondo features has also been observed for TCNQ molecules adsorbed on Au(111) and has been attributed to the competition between the purely inelastic channel and the one including the Kondo effect.[41]

C. Inelastic triplet-singlet and Kondo excitations

In contrast to the spectra of the TM ions, the spectrum of NiPc recorded on benzene does not present signatures of finite-bias excitations. The CuPc benzene spectrum, however, presents two side peaks at $\pm 21 \pm 1$ meV, shown in Fig. 9(b). These side peaks are assigned to intramolecular magnetic excitations,[7] due to the presence of two spins in CuPc, one in the $d_{x^2-y^2}$ (b_{1g}) state localized on the Cu[32] and the other in the $2e_g$ ligand state. This interpretation is supported by the gas-phase calculation of charged molecules presented later. The energy of the side peaks provides a direct estimate of the intramolecular exchange coupling (J) between d and π spins. The observation of an intense Kondo peak at zero bias, on the other hand, indicates that the CuPc ground state is magnetic, namely a triplet ($S = 1$) state where the metal and ligand spins are aligned parallel to each other, whereas the excited state is a singlet ($S = 0$) state.

The similarity between the elastic Kondo resonances of NiPc and CuPc, with $S = 1/2$ and $S = 1$, respectively, can be explained by the fact that the total CuPc spin is underscreened due to the very weak coupling between the b_{1g} ($d_{x^2-y^2}$) orbital and the substrate. Indeed, the ratio between the degree of hybridization with the substrate obtained for $2e_g$ and b_{1g} in the DFT calculations presented in the next chapter results in a negligible $T_K \sim 10^{-22}$ K for the Kondo effect of b_{1g}. Thus, only the $2e_g$ ligand spin is effectively screened by the substrate in the temperature range accessible by our STM.

D. Multiorbital noncrossing approximation of the Kondo resonance associated to the ligand spin

Although spin excitations coupled to the Kondo effect have already been observed in transport experiments with molecular junctions,[39,73,82–84] the precise configuration of the molecule-metal bonding provided by STM and the assignment of the Kondo-screened spin to a specific orbital allow us to model our results by mapping the electronic structure of CuPc/Ag(100) calculated by DFT onto an impurity Hamiltonian. Our model describes the interaction between the $2e_g$ orbital and the substrate by an SU(4) Anderson Hamiltonian, where twofold spin degeneracy coexists with the twofold orbital degeneracy on the same footing and an infinite repulsive Coulomb term (see Ref. 86 for more details). DFT calculations show that the interaction between the ion b_{1g} state and the substrate can be neglected, as reflected by the small hybridization-induced broadening obtained for this orbital, which is a factor of 20 smaller than that of the $2e_g$ state. The Hamiltonian includes a molecular exchange term $-J S_L S_{TM}$, which couples the ligand spin (S_L) to the TM spin (S_{TM}). The $2e_g$ on-site energy is fitted to $\epsilon = -0.35$ eV, and the spectral density of the coupling with the substrate is assumed to have rectangular shape with magnitude $\Gamma = 0.1$ eV and band half-width of 10 eV.

The PDOS onto the $2e_g$ state, calculated within the noncrossing approximation at $T = 5$ K (see Ref. 86), is compared with the experimental dI/dV spectra in Fig. 9(b). For STM studies this comparison is a first-order approximation that takes into account that the tunneling conductance is proportional to the local DOS. Moreover, our calculations are performed in equilibrium. At typical STM parameters, the nonequilibrium modification of NCA equations[87] for slowly varying substrate DOS reduce to corrections smaller than $1/1000^{\mathrm{th}}$ in the tunneling current. Hence, in these STM studies, the equilibrium spectral function is an excellent approximation to compare with the experiment. This is confirmed by the correct reproduction of the Kondo features observed for NiPc and CuPc when we set the intramolecular coupling term to 0 and 25 meV, respectively, as shown in the bottom graph of Fig. 9(b). In the case of ferromagnetic coupling, the finite-bias features correspond to inelastic Kondo replicas that originate from spin excitations. Decomposition into spin channels yields that the Stokes satellite (positive bias) is in the $S = 0$ channel, whereas the anti-Stokes peak (negative bias) as well as the Kondo peak are in the $S = 1$ channel.[86,88]

E. Magnetic moments calculated by DFT

By calculating the saturation magnetic moments of TMPc, DFT provides complementary results to the analysis of the Kondo spectra reported above. Moreover, in addition to supporting the interpretation of the STS data, DFT allows us to construct a quantitative picture of the effect of the different charge transfer mechanisms on the molecular magnetic properties. Table II summarizes the magnetic moments calculated for the neutral and anionic form of gas-phase TMPc as well as for TMPc adsorbed on Ag(100). We notice that, although the amount of charge transferred from the substrate to the molecules is similar in all cases, the total magnetic moment is reduced in FePc and CoPc, whereas it is increased in NiPc and CuPc with respect to the neutral gas-phase TMPc. The calculations confirm that the magnetic moment of the TM ions in NiPc and CuPc is not perturbed upon adsorption, due to the small hybridization of the planar b_{1g} orbital with the substrate states. This is in agreement with previous results obtained by XMCD on CuPc/Ag(100) (Ref. 32) and with the coexistence of TM and ligand spins in CuPc inferred from the Kondo spectra. We recall that, due to the underestimation of correlation effects in DFT, the ligand spin is just barely present in the calculations with adsorbates. For NiPc, we calculate a small magnetic moment of 0.14 μ_B, while for CuPc the moment is just slightly larger than the 1 μ_B corresponding to the unpaired spin in the b_{1g} orbital. Since charge transfer is close to one electron, one way to estimate the magnitude of the ligand spin using DFT is to consider gas-phase anions as a proxy of adsorbed TMPc. In such a case the number of electrons belonging to the molecule is fixed and the calculations can be constrained to yield the minimum energy spin state. Figure 10 displays the spin density of neutral and anionic gas-phase molecules, where we clearly observe the additional ligand spin of NiPc and CuPc after charge transfer. In CuPc, the spin density originating from the b_{1g} orbital is also observed, distributed over the Cu ion and N_p atoms.

FePc and CoPc present a more complicate picture compared to the simple addition of one spin in NiPc and CuPc, partly because of the strong hybridization with the substrate discussed in Sec. V B. In both cases, the magnetic moment is reduced upon adsorption. The extra electron donated by the surface is not easily assigned to a single MO, inducing

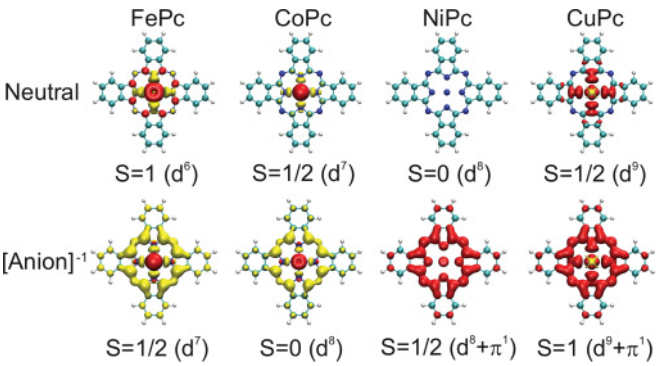

FIG. 10. (Color online) Spin density of neutral (top) and anionic (bottom) gas-phase TMPc in D_{4h} symmetry. Red (yellow) indicate spin up (down). The isovalue for the spin density is 0.005 $e^-/\text{Å}^3$.

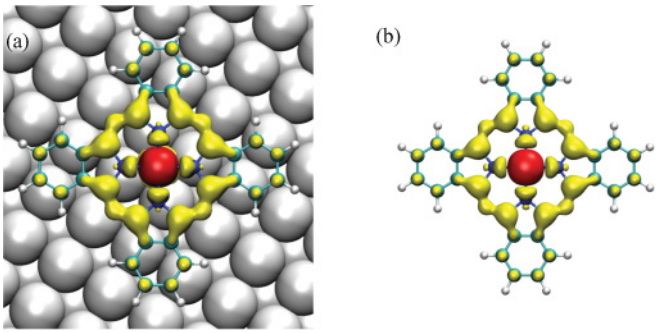

FIG. 11. (Color online) Spin-density distribution of FePc (a) adsorbed on Ag(100) and (b) in the gas-phase anion. Red/yellow denote spin up/down. The isovalue for the spin density is 0.005 $e^-/\text{Å}^3$ in both cases.

a reorganization of the charge within the molecule. We use the results obtained for gas-phase anions to disentangle the different mechanisms responsible for the quenching of the magnetic moment. As shown in Fig. 11, the spin density of FePc follows the same distribution in the gas-phase anion and in the adsorbed molecule. This similarity can also be checked by comparing their element-resolved magnetic moments in Table III, which are very similar in both cases. Thus, regardless of the strong hybridization of adsorbed FePc, the main features of the spin moment distribution are again captured by the simple addition of one electron to the gas-phase system. The true nature of the ground state of FePc on Ag (100), however, might be more complex than suggested by the calculated spin-density distribution, due to the interplay of several MO close to E_F and dynamic electron correlation effects that are not included in DFT. The computed electronic structure for FePc yields a $S = 1/2$ system when adsorbed on Ag(100), same as for the gas-phase anion. However, the adsorbate exhibits a more complex configuration due to the presence of multiple molecular orbitals at the Fermi level. This could result in either a mixed-valence system, given the Fermi level crossing and strong interaction of the a_{1g} orbital with the substrate, or a more complex Kondo behavior with a low-temperature Kondo phase originating in the many less-coupled orbitals near the Fermi energy. This complex behavior makes FePc/Ag(100) an interesting candidate to study very low temperature Kondo physics in a multiorbital system.

CoPc represents another case of nontrivial charge transfer occurring upon adsorption. For example, the a_{1g} orbital is filled, but new empty d_π states appear above E_F, as shown in Figs. 4(b) and 4(c). Moreover, the anion is not a good model for the adsorbed molecule. As shown in Table II and Fig. 10, the anion is in a $S = 0$ state, due to antiferromagnetic coupling

TABLE III. Computed element-resolved magnetic moment m (units of μ_B) for FePc in the neutral and anionic gas phase, and in the adsorbate, using GGA + U.

	m_M	m_N	m_C	m_{tot}
FePc_{gas}	1.94	−0.13	0.19	2.00
$[\text{FePc}]^{1-}_{\text{gas}}$	2.04	−0.31	−0.73	1.00
$\text{FePc}_{\text{Ag(100)}}$	2.14	−0.26	−0.82	1.06

between spins residing in different MOs, while in the adsorbed case we find a noninteger spin magnetic moment of 0.63 μ_B. This noninteger spin, together with the absence of a Kondo interaction, could indicate that CoPc is in the mixed-valence regime, with charge fluctuating between the CoPc d and Ag states, similarly to results obtained for CoPc on Au(111) using x-ray absorption spectroscopy.[3]

F. Intramolecular exchange coupling

The TM-ligand spin coupling observed via the inelastic Kondo interaction in CuPc can be studied in gas-phase $[CuPc]^{1-}$. Here, the energy of ferromagnetic and antiferromagnetic spin configurations can be computed by fixing the total spin of the molecule. The ferromagnetic (triplet) alignment is favored over the antiferromagnetic (singlet) one. The triplet ground state is in agreement with the zero-bias Kondo resonance observed experimentally. From the energy difference between triplet and singlet states, evaluated using the parallel spin ($E_{\uparrow\uparrow}$) and antiparallel spin ($E_{\uparrow\downarrow}$) energies, and taking the correct singlet and triplet configurations to yield $J = 2(E_{\uparrow\downarrow} - E_{\uparrow\uparrow})$, we extract the exchange coupling constant J for the anion, $J = 38$ meV. The discrepancy with $J = 21$ meV measured for CuPc/Ag(100) can be explained by surface screening, which is expected to significantly reduce exchange correlation effects involving hybridized orbitals.

The distribution of the spin density in $[FePc]^{1-}$ and $[CoPc]^{1-}$, shown in Fig. 10, reveals a different type of intramolecular spin correlation. Both neutral and anionic molecules exhibit antiferromagnetically aligned TM and ligand spins, indicating that the spin contrast is not directly due to the interaction with the substrate but is intrinsic to the molecule and related to the pristine TM spin, which extends to nearby C and N atoms after the formation of MOs with mixed d and π character. Such intramolecular antiferromagnetic spin coupling is a result of the large exchange splitting of the d levels of the Fe and Co ions. This induces spin-dependent mixing of the d and ligand states, leading to the formation of spin-polarized MOs with different spatial distribution. A similar mechanism can be invoked to explain the site- and energy-dependent spin contrast recently measured for CoPc deposited on Fe(110), for which the total molecular moment is zero.[23]

VII. CONCLUSIONS

The adsorption, electronic, and magnetic structure of four TMPc (M = Fe, Co, Ni, and Cu) adsorbed on Ag(100) have been systematically studied using STM, STS, and *ab initio* DFT calculations within the LDA, GGA, GGA + vdW, and GGA + U approximations.

We find that all molecules adsorb with the macrocycle plane parallel to the surface and the TM-N_p ligand axis rotated by $\pm 30^\circ$ with respect to the high-symmetry surface lattice vectors. The comparison between DFT results using different approximations evidences differences in the TM-Ag interaction, but the leading role of vdW forces leads to similar molecule-substrate distances and azimuthal rotation angles. The rotation between molecular and surface symmetry axes imprints chirality to the frontier electronic orbitals without perturbing the structural conformation of the molecules. This can be observed only in NiPc and CuPc at negative voltages, due to the contribution of the a_{1u} and partially occupied $2e_g$ orbitals to the tunneling current and minor influence of the d channels in the same energy region.

The electronic structure of adsorbed TMPc is modified mainly due to charge transfer from the substrate. Although all molecules receive approximately one electron, charge is transferred to the ligand $2e_g$ orbital in NiPc and CuPc, and to multiple MOs in FePc and CoPc, inducing internal charge reorganization. This difference is related to both energy-level alignment and Coulomb repulsion. In addition, whereas FePc and CoPc exhibit strongly hybridized $d_\perp$ states near E_F, those are shifted down in energy in NiPc and CuPc, which display unperturbed $d_\parallel$ states in this energy range. The electronic configuration of the Ni and Cu ions is not significantly affected by adsorption.

Both charge transfer and hybridization tend to reduce the magnetic moment of FePc and CoPc. The computed electronic structure of FePc indicates a $S = 1/2$ system when adsorbed on Ag(100), with a strong presence of MOs near the Fermi energy that could indicate either a mixed-valence system, given the strong interaction of the a_{1g} orbital with the substrate, or a more complex Kondo behavior with a low-temperature Kondo phase originating in the many less-coupled orbitals near the Fermi energy. The noninteger moment obtained for CoPc and the existence of a substantial molecular DOS at the Fermi energy (see Fig. 4), together with the absence of a Kondo resonance in this molecule, suggests a mixed-valence configuration. Opposite to the moment reduction in FePc and CoPc, the spin multiplicity is actually enhanced by charge transfer in NiPc and CuPc, due to the induction of a ligand spin in the $2e_g$ orbital. This transforms NiPc into a paramagnetic molecule and induces a triplet ground state in CuPc, where the ligand spin is exchange coupled to the TM magnetic moment.

The interaction between the $2e_g$ ligand spin of NiPc and CuPc and the substrate gives rise to a Kondo interaction, which induces a prominent zero bias resonance delocalized over the perimeter of the molecules. Coherent coupling between Kondo spin flip and vibrational excitations induces inelastic Kondo resonances in both NiPc and CuPc. In CuPc, the total magnetic moment is underscreened as the Kondo energy scale of the TM spin is orders of magnitude smaller than the one of the $2e_g$ ligand spin. However, the additional magnetic degree of freedom due to the TM spin leads to the coupling of Kondo and inelastic triplet-singlet excitations. The coexistence of different nonequilibrium Kondo processes related to vibrational and spin transitions in CuPc opens up the possibility to study the time scale and spatial localization of multiple spin excitation and relaxation channels within a single molecule, as reported in more detail in Ref. 7.

In general, we show that charge transfer and hybridization of MOs orbitals have profound effects on the electronic configuration, magnetic moment, and transport properties of metal-organic complexes adsorbed on a metallic substrate. Such effects in TMPc do not depend monotonically on the

electronic configuration of the TM ions. Rather, the energy position, symmetry, and spin polarization of the pristine MOs has to be considered within a comprehensive picture of the charge transfer process. Importantly, the magnetic moment of adsorbed TMPc can be either reduced or enhanced depending on the relative energy of the $d_\perp$ and π levels, and their degree of hybridization with the substrate. Further, the possibility of inducing additional ligand spins upon adsorption may be relevant to establish magnetic coupling in extended molecular structures assembled on metal surfaces.

ACKNOWLEDGMENTS

We acknowledge support from the European Research Council (StG 203239 NOMAD), Ministerio de Ciencia e Innovación (MAT2010-15659), and Agència de Gestió d'Ajuts Universitaris i de Recerca (2009 SGR 695). A.M. acknowledges funding from the Ramon y Cajal Fellowship program. R.R. is supported by a JAE-Doc contract from the Consejo Superior de Investigaciones Científicas. R.R., R.K., and N.L. have been supported by the ICT-FET Integrated Project AtMol (http://www.atmol.eu).

[1] D. Heim, K. Seufert, W. Auwaìrter, C. Aurisicchio, C. Fabbro, D. Bonifazi, and J. V. Barth, Nano Lett. **10**, 122 (2010).
[2] A. Mugarza, N. Lorente, P. Ordejón, C. Krull, S. Stepanow, M.-L. Bocquet, J. Fraxedas, G. Ceballos, and P. Gambardella, Phys. Rev. Lett. **105**, 115702 (2010).
[3] S. Stepanow, P. S. Miedema, A. Mugarza, G. Ceballos, P. Moras, J. C. Cezar, C. Carbone, F. M. F. de Groot, and P. Gambardella, Phys. Rev. B **83**, 220401 (2011).
[4] Y. Xue and M. A. Ratner, Phys. Rev. B **68**, 115406 (2003).
[5] K. Moth-Poulsen and T. Björnholm, Nat. Nanotechnol. **4**, 551 (2009).
[6] O. Bekaroglu, Y. Bian, G. Bottari, X. Cai, G. de la Torre, U. Hahn, N. Ishikawa, J. Jiang, N. Kobayashi, X. Li *et al.*, *Functional Phthalocyanine Molecular Materials* (Springer, Berlin, 2010).
[7] A. Mugarza, C. Krull, R. Robles, S. Stepanow, G. Ceballos, and P. Gambardella, Nat. Commun. **2**, 490 (2011).
[8] S.-H. Chang, S. Kuck, J. Brede, L. Lichtenstein, G. Hoffmann, and R. Wiesendanger, Phys. Rev. B **78**, 233409 (2008).
[9] G. Dufour, C. Poncey, F. Rochet, H. Roulet, S. Iacobucci, M. Sacchi, F. Yubero, N. Motta, M. Piancastelli, A. Sgarlata *et al.*, J. Electron. Spectrosc. Relat. Phenom. **76**, 219 (1995).
[10] Y. Wang, J. Kröger, R. Berndt, and W. Hofer, Angew. Chem. **121**, 1287 (2009).
[11] M. Kanai, T. Kawai, K. Motai, X. Wang, T. Hashizume, and T. Sakura, Surf. Sci. **329**, L619 (1995).
[12] L. Liu, J. Yu, N. O. Viernes, J. S. Moore, and J. W. Lyding, Surf. Sci. **516**, 118 (2002).
[13] D. G. de Oteyza, A. El-Sayed, J. M. García-Lastra, E. Goiri, T. N. Krauss, A. Turak, E. Barrena, H. Dosch, J. Zegenhagen, A. Rubio *et al.*, J. Chem. Phys. **133**, 214703 (2010).
[14] L. Gao, W. Ji, Y. B. Hu, Z. H. Cheng, Z. T. Deng, Q. Liu, N. Jiang, X. Lin, W. Guo, S. X. Du *et al.*, Phys. Rev. Lett. **99**, 106402 (2007).
[15] N. Tsukahara, K. ichi Noto, M. Ohara, S. Shiraki, N. Takagi, Y. Takata, J. Miyawaki, M. Taguchi, A. Chainani, S. Shin *et al.*, Phys. Rev. Lett. **102**, 167203 (2009).
[16] N. Tsukahara, S. Shiraki, S. Itou, N. Ohta, N. Takagi, and M. Kawai, Phys. Rev. Lett. **106**, 187201 (2011).
[17] R. Cuadrado, J. I. Cerdá, Y. Wang, G. Xin, R. Berndt, and H. Tang, J. Chem. Phys. **133**, 154701 (2010).
[18] M. Takada and H. Tada, Ultramicroscopy **105**, 22 (2005).
[19] A. Zhao, Q. Li, L. Chen, H. Xiang, W. Wang, S. Pan, B. Wang, X. Xiao, J. Yang, J. G. Hou *et al.*, Science **309**, 1542 (2005).
[20] Z. Li, B. Li, J. Yang, and J. G. Hou, Acc. Chem. Res. **43**, 954 (2010).
[21] B. W. Heinrich, C. Iacovita, T. Brumme, D.-J. Choi, L. Limot, M. V. Rastei, W. A. Hofer, J. Kortus, and J.-P. Bucher, J. Phys. Chem. Lett.**1**, 1517 (2010).
[22] C. Iacovita, M. V. Rastei, B. W. Heinrich, T. Brumme, J. Kortus, L. Limot, and J. P. Bucher, Phys. Rev. Lett. **101**, 116602 (2008).
[23] J. Brede, N. Atodiresei, S. Kuck, P. Lazić, V. Caciuc, Y. Morikawa, G. Hoffmann, S. Blügel, and R. Wiesendanger, Phys. Rev. Lett. **105**, 047204 (2010).
[24] Y.-S. Fu, S.-H. Ji, X. Chen, X.-C. Ma, R. Wu, C.-C. Wang, W.-H. Duan, X.-H. Qiu, B. Sun, P. Zhang *et al.*, Phys. Rev. Lett. **99**, 256601 (2007).
[25] X. Chen, Y.-S. Fu, S.-H. Ji, T. Zhang, P. Cheng, X.-C. Ma, X.-L. Zou, W.-H. Duan, J.-F. Jia, and Q.-K. Xue, Phys. Rev. Lett. **101**, 197208 (2008).
[26] P. Gargiani, M. Angelucci, C. Mariani, and M. G. Betti, Phys. Rev. B **81**, 085412 (2010).
[27] F. Evangelista, A. Ruocco, R. Gotter, A. Cossaro, L. Floreano, A. Morgante, F. Crispoldi, M. G. Betti, and C. Mariani, J. Chem. Phys. **131**, 174710 (2009).
[28] A. Ruocco, F. Evangelista, R. Gotter, A. Attili, and G. Stefani, J. Phys. Chem. C **112**, 2016 (2008).
[29] H. Peisert, M. Knupfer, and J. Fink, Surf. Sci. **515**, 491 (2002).
[30] F. Petraki, H. Peisert, I. Biswas, U. Aygül, F. Latteyer, A. Vollmer, and T. Chassé, J. Phys. Chem. Lett. **1**, 3380 (2010).
[31] E. Annese, J. Fujii, I. Vobornik, G. Panaccione, and G. Rossi, Phys. Rev. B **84**, 174443 (2011).
[32] S. Stepanow, A. Mugarza, G. Ceballos, P. Moras, J. C. Cezar, C. Carbone, and P. Gambardella, Phys. Rev. B **82**, 014405 (2010).
[33] Y. Y. Zhang, S. X. Du, and H.-J. Gao, Phys. Rev. B **84**, 125446 (2011).
[34] X. Chen and M. Alouani, Phys. Rev. B **82**, 094443 (2010).
[35] J. D. Baran, J. A. Larsson, R. A. J. Woolley, Y. Cong, P. J. Moriarty, A. A. Cafolla, K. Schulte, and V. R. Dhanak, Phys. Rev. B **81**, 075413 (2010).
[36] Z. Hu, B. Li, A. Zhao, J. Yang, and J. G. Hou, J. Phys. Chem. C**112**, 13650 (2008).
[37] T. Komeda, H. Isshiki, J. Liu, Y.-F. Zhang, N. Lorente, K. Katoh, B. K. Breedlove, and M. Yamashita, Nat. Commun. **2**, 217 (2011).
[38] A. Lodi Rizzini, C. Krull, T. Balashov, J. J. Kavich, A. Mugarza, P. S. Miedema, P. K. Thakur, V. Sessi, S. Klyatskaya, M. Ruben *et al.*, Phys. Rev. Lett. **107**, 177205 (2011).
[39] E. A. Osorio, K. Moth-Poulsen, H. S. J. van der Zant, J. Paaske, P. Hedegaard, K. Flensberg, J. Bendix, and T. Björnholm, Nano Lett. **10**, 105 (2010).

[40]U. G. E. Perera, H. J. Kulik, V. Iancu, L. G. G. V. Dias da Silva, S. E. Ulloa, N. Marzari, and S. W. Hla, Phys. Rev. Lett. **105**, 106601 (2010).
[41]I. Fernández-Torrente, K. J. Franke, and J. I. Pascual, Phys. Rev. Lett. **101**, 217203 (2008).
[42]P. Wahl, L. Diekhoner, M. A. Schneider, and K. Kern, Rev. Sci. Instrum. **79**, 043104 (2008).
[43]I. Horcas, R. Fernández, J. M. Gómez-Rodríguez, J. Colchero, J. Gómez-Herrero, and A. M. Baro, Rev. Sci. Instrum. **78**, 013705 (2007).
[44]G. Kresse and D. Joubert, Phys. Rev. B **59**, 1758 (1999).
[45]G. Kresse and J. Furthmüller, Comput. Mater. Sci. **6**, 15 (1996).
[46]J. P. Perdew and A. Zunger, Phys. Rev. B **23**, 5048 (1981).
[47]J. P. Perdew, K. Burke, and M. Ernzerhof, Phys. Rev. Lett. **77**, 3865 (1996).
[48]S. Grimme, J. Comput. Chem. **27**, 1787 (2006).
[49]T. Bucko, J. Hafner, S. Lebegue, and J. G. Angyan, J. Phys. Chem. A **114**, 11814 (2010).
[50]S. L. Dudarev, G. A. Botton, S. Y. Savrasov, C. J. Humphreys, and A. P. Sutton, Phys. Rev. B **57**, 1505 (1998).
[51]R. F. W. Bader, W. H. Henneker, and P. E. Cade, J. Chem. Phys. **46**, 3341 (1967).
[52]W. Tang, E. Sanville, and G. Henkelman, J. Phys.: Condens. Matter **21**, 084204 (2009).
[53]B. Thole, G. V. D. Laan, and P. Butler, Chem. Phys. Lett. **149**, 295 (1988).
[54]B. W. Dale, R. J. P. Williams, C. E. Johnson, and T. L. Thorp, J. Chem. Phys. **49**, 3441 (1968).
[55]P. A. Reynolds and B. N. Figgis, Inorg. Chem. **30**, 2294 (1991).
[56]M.-S. Liao and S. Scheiner, J. Chem. Phys. **114**, 9780 (2001).
[57]M. D. Kuzmin, R. Hayn, and V. Oison, Phys. Rev. B **79**, 024413 (2009).
[58]N. Marom and L. Kronik, Appl. Phys. A **95**, 159 (2009).
[59]F. Roth, A. König, R. Kraus, M. Grobosch, T. Kroll, and M. Knupfer, Eur. Phys. J. B **74**, 339 (2010).
[60]X. Lu, K. W. Hipps, X. D. Wang, and U. Mazur, J. Am. Chem. Soc. **118**, 7197 (1996).
[61]P. H. Lippel, R. J. Wilson, M. D. Miller, C. Wöll, and S. Chiang, Phys. Rev. Lett. **62**, 171 (1989).
[62]J. D. Sau, J. B. Neaton, H. J. Choi, S. G. Louie, and M. L. Cohen, Phys. Rev. Lett. **101**, 026804 (2008).
[63]A. Greuling, M. Rohlfing, R. Temirov, F. S. Tautz, and F. B. Anders, Phys. Rev. B **84**, 125413 (2011).
[64]J. Gores, D. Goldhaber-Gordon, S. Heemeyer, M. A. Kastner, H. Shtrikman, D. Mahalu, and U. Meirav, Phys. Rev. B **62**, 2188 (2000).
[65]V. Madhavan, W. Chen, T. Jamneala, M. F. Crommie, and N. S. Wingreen, Science **280**, 567 (1998).
[66]V. Mantsevich and N. Maslova, Solid State Commun. **150**, 2072 (2010).
[67]D. M. Kolb, W. Boeck, K.-M. Ho, and S. H. Liu, Phys. Rev. Lett. **47**, 1921 (1981).
[68]A. J. Cohen, P. Mori-Sánchez, and W. Yang, Science **321**, 792 (2008).
[69]R. W. I. de Boer, A. F. Stassen, M. F. Craciun, C. L. Mulder, A. Molinari, S. Rogge, and A. F. Morpurgo, Appl. Phys. Lett. **86**, 262109 (2005).
[70]A. C. Hewson, *The Kondo Problem to Heavy Fermions* (Cambridge University Press, Cambridge, UK, 1993).
[71]M. Ternes, A. J. Heinrich, and W.-D. Schneider, J. Phys.: Condens. Matter **21**, 053001 (2009).
[72]K. Nagaoka, T. Jamneala, M. Grobis, and M. F. Crommie, Phys. Rev. Lett. **88**, 077205 (2002).
[73]J. J. Parks, A. R. Champagne, T. A. Costi, W. W. Shum, A. N. Pasupathy, E. Neuscamman, S. Flores-Torres, P. S. Cornaglia, A. A. Aligia, C. A. Balseiro *et al*., Science **328**, 1370 (2010).
[74]D. Goldhaber-Gordon, J. Gores, M. A. Kastner, H. Shtrikman, D. Mahalu, and U. Meirav, Phys. Rev. Lett. **81**, 5225 (1998).
[75]B. C. Stipe, M. A. Rezaei, and W. Ho, Science **280**, 1732 (1998).
[76]N. Lorente and J.-P. Gauyacq, Phys. Rev. Lett. **103**, 176601 (2009).
[77]M. N. Kiselev, Phys. Status Solidi C **4**, 3362 (2007).
[78]G. P. Lansbergen, G. C. Tettamanzi, J. Verduijn, N. Collaert, S. Biesemans, M. Blaauboer, and S. Rogge, Nano Lett. **10**, 455 (2010).
[79]J. Paaske and K. Flensberg, Phys. Rev. Lett. **94**, 176801 (2005).
[80]L. H. Yu, Z. K. Keane, J. W. Ciszek, L. Cheng, M. P. Stewart, J. M. Tour, and D. Natelson, Phys. Rev. Lett. **93**, 266802 (2004).
[81]T. Choi, S. Bedwani, A. Rochefort, C.-Y. Chen, A. J. Epstein, and J. A. Gupta, Nano Lett. **10**, 4175 (2010).
[82]A. Kogan, G. Granger, M. A. Kastner, D. Goldhaber-Gordon, and H. Shtrikman, Phys. Rev. B **67**, 113309 (2003).
[83]J. Paaske, A. Rosch, P. Wölfle, N. Mason, C. M. Marcus, and J. Nygaard, Nat. Phys. **2**, 460 (2006).
[84]N. Roch, S. Florens, V. Bouchiat, W. Wernsdorfer, and F. Balestro, Nature **453**, 633 (2008).
[85]D. Li, Z. Peng, L. Deng, Y. Shen, and Y. Zhou, Vib. Spectrosc. **39**, 191 (2005).
[86]R. Korytar and N. Lorente, J. Phys.: Condens. Matter **23**, 355009 (2011).
[87]M. H. Hettler, J. Kroha, and S. Hershfield, Phys. Rev. B **58**, 5649 (1998).
[88]P. Roura Bas and A. A. Aligia, Phys. Rev. B **80**, 035308 (2009).